Biomed Eng Lett (2015) 5:311-320
DOI 10.1007/s13534-015-0208-9

ORIGINAL ARTICLE

Classification of Magnetic Resonance Brain Images using Bi-dimensional Empirical Mode Decomposition and Autoregressive Model

Omkishor Sahu, Vijay Anand, Vivek Kanhangad and Ram Bilas Pachori

Received: 25 July 2015 / Revised: 10 October 2015 / Accepted: 13 November 2015

Abstract
Purpose Automated classification of brain magnetic resonance (MR) images has been an extensively researched topic in biomedical image processing. In this work, we propose a new approach for classifying normal and abnormal brain MR images using bi-dimensional empirical mode decomposition (BEMD) and autoregressive (AR) model.
Methods In our approach, brain MR image is decomposed into four intrinsic mode functions (IMFs) using BEMD and AR coefficients from multiple IMFs are concatenated to form a feature vector. Finally a binary classifier, least-squares support vector machine (LS-SVM), is employed to discriminate between normal and abnormal brain MR images.
Results The proposed technique achieves 100% classification accuracy using second-order AR model with linear and radial basis function (RBF) as kernels in LS-SVM.
Conclusions Experimental results confirm that the performance of the proposed method is quite comparable with the existing results. Specifically, the presented approach outperforms one-dimensional empirical mode decomposition (1D-EMD) based classification of brain MR images.

Keywords Magnetic resonance imaging (MRI), Bi-dimensional empirical mode decomposition (BEMD), Intrinsic mode function (IMF), Autoregressive (AR) model

INTRODUCTION

Magnetic resonance imaging (MRI) is commonly used method for investigating brain abnormalities [1]. Images of brain with some abnormalities are characterised by abrupt changes in image textures. For example, cancer in brain magnetic resonance image is characterised by large cells with high contrast [2], thus making it feasible to differentiate them from normal brain magnetic resonance images. Alzheimer's disease [3] is the common cause of age-related dementia. Multiple sclerosis [4] is a neurological disorder that results in various dysfunctions. Other abnormalities related to the brain include glioma, herpes encephalitis and metastatic bronchogenic carcinoma etc. [5-7]. Images of brain having above mentioned diseases are characterized by large cells and high contrast. Many methods have been proposed in the literature to identify brain magnetic resonance (MR) images having aforementioned abnormalities. Abnormal images may have one or multiple abnormalities.

Generally, the classification of medical images is performed using a two-step procedure. In first step, discriminating information or features are extracted from medical images. In the second step, a classifier utilizes the extracted information to form a decision on the category of the input image. Classification approaches are of two types, supervised and unsupervised. Supervised methods include support vector machines (SVM) [5, 8], artificial neural networks (ANN) [6] and *k*-nearest neighbor (*k*-NN) [9]. Unsupervised classification techniques include self-organization map (SOM) [5, 8] and fuzzy *c*-means [10]. Supervised methods are more common than unsupervised methods because they usually provide better accuracies [11].

In recent years, extensive research has been done in the area of automated classification of MR images of normal and abnormal brain. Two-dimensional discrete wavelet transform (2D-DWT) based approaches have been extensively explored for classification of brain MR images. Specifically, the approaches presented in [5, 12] explored approximation

Omkishor Sahu, Vijay Anand, Vivek Kanhangad (✉), Ram Bilas Pachori
Discipline of Electrical Engineering, Indian Institute of Technology Indore, Indore 452017, India
Tel : +123-45-678910 / Fax : +123-45-678910
E-mail : kvivek@iiti.ac.in

coefficients at level 2 and level 3 for discrimination, while the work in [13] presented an approach based on 2D-DWT for feature extraction, principal component analysis (PCA) for feature space reduction and back propagation neural network for classification of MR images. In another related work [14], generalized autoregressive conditional heteroscedasticity (GARCH) was employed to model wavelet coefficients of detail sub-bands. Authors in [8] used the coefficients of the approximation sub-band of two-level 2D-DWT of brain MRI as features, and SOM based neural network and SVM for classification. Maitra *et al*. [15] applied slantlet transform on intensity histogram of the image and employed back-propagation neural network (BPNN) for classification. Authors in [6] proposed a method for brain MR image classification using wavelet transform and PCA. Scaled conjugate gradient was used for optimal weight setting in BPNN for classification. Saritha *et al*. [16] used wavelet entropy based spider web plots for feature extraction and probabilistic neural network for classification to achieve maximum classification accuracy. In [17], authors proposed a three-stage approach for brain MR image classification using features extracted from LH and HL sub-bands of two level 2D-DWT with ensemble classifier. Subsequently, authors in [7] employed 2D-DWT followed by Gabor filter banks on HH sub-band of 2D-DWT for feature extraction and SVM for classification. Lahmiri *et al*. [18] employed one-dimensional empirical mode decomposition (1D-EMD) to generate intrinsic mode functions (IMFs) from brain MR images, conversion of brain MR image to one dimensional signal is done by concatenating successive rows of the image from left to right and top to bottom. Statistical features were extracted from the IMFs and an entropy based selection process was employed to identify the most informative features from each IMF followed by SVM for classification. A detailed survey of computer aided diagnosis of human brain tumor using MR images is presented in [19]. Authors in [19] also proposed a new approach employing the feedback pulse coded neural network for image segmentation followed by discrete wavelet transform (DWT) and PCA for feature extraction and forward BPNN for classification.

In the presented work, we have developed an approach for classification of normal and abnormal brain MR images. Based on our knowledge, this is the first time that bi-dimensional empirical mode decomposition (BEMD) is applied for classification of brain MR images. Experimental results show that the proposed approach has outperformed existing approaches in terms of classification accuracy.

METHODOLOGY

The classification of brain MR images is carried out in a three-step process. Firstly, BEMD is used to decompose the image into the IMFs. This is followed by modelling of individual IMFs using AR model to generate feature vectors in the form of AR coefficients. Finally, based on the extracted features least-squares support vector machine (LS-SVM) makes a decision as to whether the input brain MR image is of normal or abnormal human brain. The schematic diagram of the proposed methodology is presented in Fig. 1.

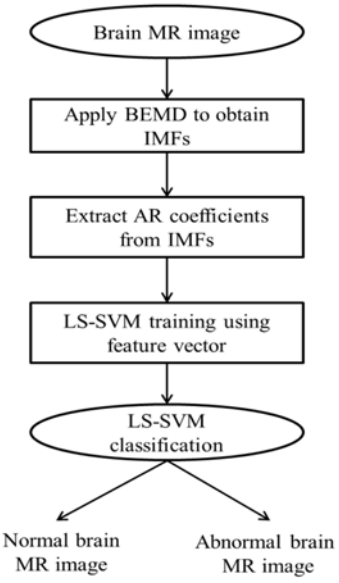

Fig. 1. Schematic diagram of the proposed approach for classification of brain MR images.

Empirical mode decomposition

Empirical mode decomposition (EMD) [20] is a multi resolution decomposition technique. EMD represents a non-stationary signal as a sum of zero-mean amplitude modulation-frequency modulation (AM-FM) components [21]. The decomposition process is adaptive and signal dependent. It is suited for the analysis of one-dimensional (1D) nonlinear and non-stationary signals. EMD decomposes a 1D signal into a set of band-limited signals called intrinsic mode functions (IMFs). The procedure used to extract IMFs from the signal is termed as sifting. The decomposition is based on the following assumptions [20, 22]:

1. The signal should have at least one maxima and one minima.
2. The time scale depends on the time interval between the extrema points.
3. If the data does not have any extrema and contains only inflection points, then it can be differentiated multiple times to obtain the extrema. The integration operation can be applied after the processing of these components.

For signal $x(t)$, sifting process can be summarized as

follows [20]:

1. Let $g(t) = x(t)$.
2. Obtain the extrema from $g(t)$.
3. Find out upper envelope $e_u(t)$ and lower envelope $e_l(t)$ by connecting maxima and minima respectively.
4. Compute the mean envelope $e_m(t)$ by averaging these two envelopes as:

$$e_m(t) = \frac{e_u(t) + e_l(t)}{2}$$

5. Subtract $e_m(t)$ from the signal $g(t)$ to generate $g(t) = g(t) - e_m(t)$.
6. Determine whether $g(t)$ is a valid IMF or not, by applying conditions of IMF.
7. If $g(t)$ is not a valid IMF, repeat steps 2 to 6 until a valid IMF is obtained.

Once a valid IMF is obtained, assign $D_1(t) = g(t)$. Obtain $r(t)$ by applying subtraction operation as $r(t) = x(t) - D_1(t)$. Replace $x(t)$ by $r(t)$ i.e. $x(t) = r(t)$. To generate the next IMF, repeat steps 2 to 7 by considering $g(t) = r(t)$. The signal $x(t)$ can now be represented as follows [20]:

$$x(t) = \sum_{i=1}^{M} D_i(t) + r_M(t) \tag{1}$$

where M represents total number of the IMFs present in the signal and $r_M(t)$ is the residual component of the signal.

EMD has been successfully applied in various areas such as electroencephalogram (EEG) signal analysis [23-29], gear fault diagnosis [30], analysis of center of pressure (COP) signals [31] and speech signal analysis [32].

Bi-dimensional empirical mode decomposition

Bi-dimensional empirical mode decomposition (BEMD) extracts two-dimensional intrinsic mode functions (2D-IMFs) during the sifting process. A 2D-IMF can be considered as a zero-mean two dimensional (2D) AM-FM component [22]. Bi-dimensional sifting process [22, 33] can be summarized as:

1. Locate the maxima and minima points of the image I by morphological reconstruction based on geodesic operators [34].
2. Interpolate the surface between all the maxima and all the minima with RBF to build the 2D envelope X_{max} and X_{min}, respectively [35].
3. Determine the mean envelope X_m by averaging the two envelopes as follows:

$$X_m = \frac{X_{max} + X_{min}}{2}$$

4. Subtract out the mean from the image to get $h_1 = \mathrm{I} - X_m$.
5. Repeat the above mentioned process till h_1 satisfy conditions of an IMF.

BEMD has applications in many areas such as texture analysis [36, 37], image denoising [38], image watermarking [39], iris recognition [40], image fusion [41], image feature extraction [42], image classification [43], texture classification and segmentation [44], etc. For our experiments, BEMD code available at MATLAB central file exchange [45] has been used.

Autoregressive model

A 2D autoregressive (AR) model for analysis of image blur using residue image of BEMD is explained in [46]. In our experiments, 2D AR model is employed on 2D-IMFs of the brain MR images. In order to analyze 2D-IMFs with 2D AR model, it is considered as a 2D random field $x[p, q]$, $(p, q) \in Z^2$.

For the $N_1 \times N_2$ image $I = \{x[p, q] : 0 \le p \le N_1 - 1, 0 \le q \le N_2 - 1\}$, 2D AR (r_1, r_2) model is defined by the following difference equation [46]:

$$x[p,q] + \sum_{i=0}^{r_1} \sum_{j=0}^{r_2} a_{ij} x[p-i, q-j] = w[p,q] \tag{2}$$

where $w[p, q]$ is a stationary white noise field with variance σ^2, r_1 and r_2 represent order of the AR model and the coefficients a_{ij} are the parameters of the 2D AR model.

In Eq. (2), the image $x[p, q]$ can be interpreted as the output of the linear time-invariant (LTI) causal system with transfer function $H(z_1, z_2)$ and a white noise as an input. The transfer function is given as [46]:

$$H(z_1, z_2) = \frac{1}{\sum_{i=0}^{r_1} \sum_{j=0}^{r_2} a_{ij} z_1^{-i} z_2^{-j}} \tag{3}$$

with $a_{00} = 1$. Assuming that the noise sequence $w[p, q]$ are known, the parameters in the AR model as described by Eq. (2) can be determined by the least-squares (LS) method as follows [46]:

$$x[p,q] + \phi^T[p,q]\theta = w[p,q] \tag{4}$$

where

$$\phi^T[p,q] = [x[p,q-1], \cdots, x[p-r_1, q-r_2]] \tag{5}$$

and

$$\theta = [a_{01}, \cdots, a_{r_1 r_2}]^T \tag{6}$$

The matrix form of Eq. (4) for $p = L + 1, ..., N_1 - 1$ and $q = M + 1, ..., N_2 - 1$ for arbitrary $L > r_1$ and $M > r_2$, provides [46]:

$$X + \Phi\theta = W \tag{7}$$

where

$$X = [x[L+1,M+1],\cdots,x[N_1-1,N_2-1]]^T,$$

$$W = [w[L+1,M+1],\cdots,w[N_1-1,N_2-1]]^T$$

and Φ is given as [46]:

$$\Phi = \begin{pmatrix} x[L+1,1] & \cdots & x[L+1-r_1,M+1-r_2] \\ x[L+2,1] & \cdots & x[L+2-r_1,M+1-r_2] \\ \vdots & \ddots & \vdots \\ x[N_1-1,N_2-1] & \cdots & x[N_1-1-r_1,N_2-1-r_2] \end{pmatrix}$$

Assuming that Φ is known, a LS estimate of the parameter vector θ in Eq. (7) can be obtained as [46]:

$$\hat{\theta} = -(\Phi^T\Phi)^{-1}\Phi^T X \tag{8}$$

AR model has been employed for many applications such as shape classification [47], EEG and electrocardiogram (ECG) signal classification [48, 49], image texture analysis [50], etc.

Least-squares support vector machine

SVM was introduced in [51]. It is based on statistical learning theory. To classify the data, SVM constructs optimal separating hyperplane which maximizes the margin between the two nearest data points which belongs to two different classes. Consider N number of data points $\{x_i, y_i\}_{i=1}^N$, where $x_i \in \mathbb{R}^d$ is d-dimension input feature and $y_i \in \{+1, -1\}$ is class label. For two class classification problem, separating hyperplane is given as [52]:

$$f(x) = \text{sign}[\Omega^T g(x) + \beta] \tag{9}$$

where Ω is n-dimensional weight vector and $g(x)$ is a mapping function that maps x into the n-dimensional space and β is a bias. The least-squares version of SVM, which is known as least-squares SVM (LS-SVM) was introduced in [52], the classification problem using LS-SVM can be formulated as [52]:

$$\min J(\Omega,\beta,\varepsilon) = \frac{1}{2}\Omega^T\Omega + \frac{\gamma}{2}\sum_{i=1}^{N}\varepsilon_i^2 \tag{10}$$

subject to the following equality constraint,

$$y_i[\Omega^T g(x_i) + \beta] = 1 - \varepsilon_i, i = 1,2,\ldots,N \tag{11}$$

where $\varepsilon = (\varepsilon_1, \varepsilon_2, \cdots, \varepsilon_N)^T$.

The Lagrangian multiplier α_i for Eq. (10) can be defined as [52]:

$$L(\Omega,\beta,\varepsilon;\alpha) = J(\Omega,\beta,\varepsilon) - \sum_{i=1}^{N}\alpha_i\{y_i[\Omega^T g(x_i)+\beta]-1+\varepsilon_i\} \tag{12}$$

On solving Eq. (12) by considering the optimal conditions, LS-SVM classifier is obtained as [52]:

$$f(x) = \text{sign}\left(\sum_{i=1}^{N}\alpha_i y_i K(x,x_i) + \beta\right) \tag{13}$$

where $K(x, x_i)$ is kernel function. In the presented work, different kernel functions have been used which are defined as follows [53]:

1. Linear kernel function:

$$K(x, x_i) = xx_i \tag{14}$$

2. Polynomial kernel function:

$$K(x, x_i) = (xx_i + 1)^d \tag{15}$$

where d is the degree of the polynomial.

3. Radial basis function (RBF) kernel:

$$K(x,x_i) = e^{\frac{-\|x-x_i\|^2}{2\sigma^2}} \tag{16}$$

where σ controls the width of RBF function.

LS-SVM has been widely used for classification of EEG signals [54, 55], ECG signals [56], electromyogram (EMG) signals [57], MR images [58], etc.

EXPERIMENTAL RESULTS AND DISCUSSION

Experimental evaluation of the proposed method was performed on a publicly available AANLIB database of Harvard medical school [59]. Fig. 2 presents a set of brain MR images from the database. For our experiments, a total of 88 axial, T2-weighted brain MR images are used, out of which 25 images correspond to normal human brain and the remaining 63 images correspond to human brain affected by diseases such as alzheimer's, glioma, herpes encephalitis, metastatic bronchogenic carcinoma and multiple sclerosis. Number of images corresponding to each of these diseases is presented in Table 1.

In our experiments, BEMD is applied on each of the brain MR images to extract 2D-IMFs. Figs. 3 and 4 show sample brain MR images and corresponding IMFs for normal and abnormal category, respectively. As can be observed from

Table 1. Distribution of abnormal brain MR images in database.

Disease	Number of images
Alzheimer's	10
Glioma	12
Herpes encephalitis	16
Metastatic bronchogenic carcinoma	11
Multiple sclerosis	14

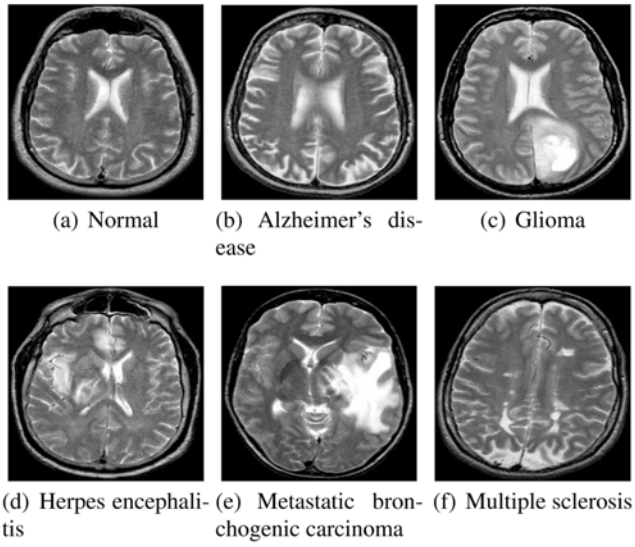

Fig. 2. Sample brain MR images in the AANLIB database.

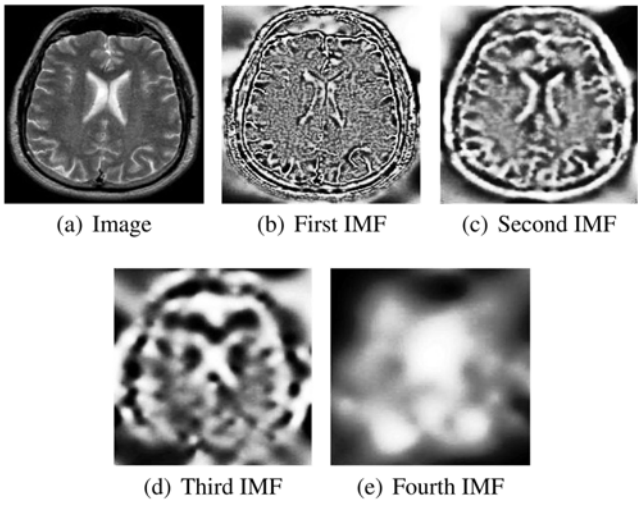

Fig. 3. Sample normal brain MR image and corresponding IMFs.

these figures, the visual information contained in 2D-IMFs decreases as the mode of 2D-IMFs is increased. Therefore, in our experiments, only the first four 2D-IMFs are used for further processing.

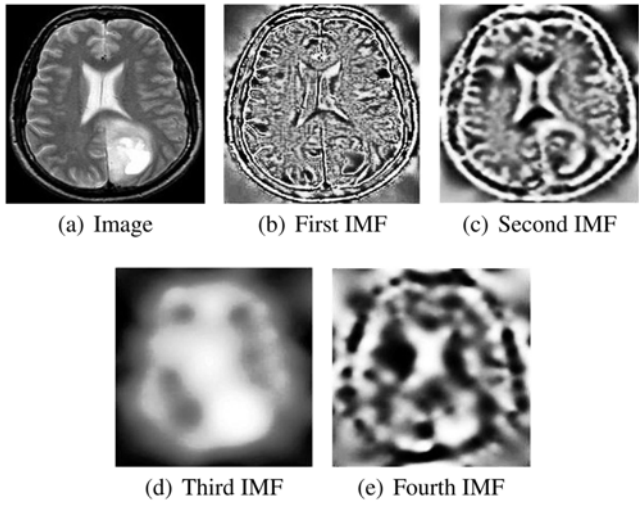

Fig. 4. Sample abnormal brain MR image and corresponding IMFs.

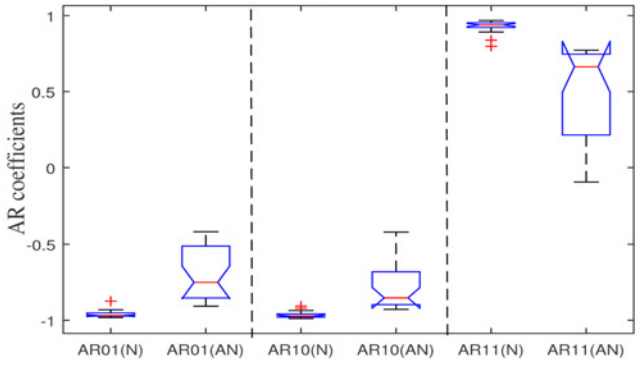

Fig. 5. Box plot of 1st order AR coefficients of normal and abnormal brain MR images.

In our approach, each of the 2D-IMF is modeled using a 2D AR model. In this way, we obtained AR coefficients for each of the IMFs, which are concatenated to form the feature vector. The class discrimination ability of AR coefficients as feature vector is quantified using Kruskal-Wallis statistical test [60]. The results are presented in Figs. 5, 6 and 7 for 1st, 2nd and 3rd order AR coefficients respectively for discrimination of normal (N) and abnormal (AN) brain MR images. Also, the *p*-values obtained from the test are presented in Table 2.

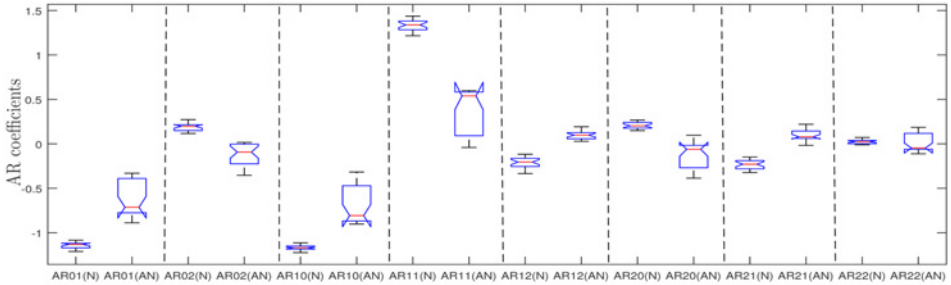

Fig. 6. Box plot of 2nd order AR coefficients of normal and abnormal brain MR images.

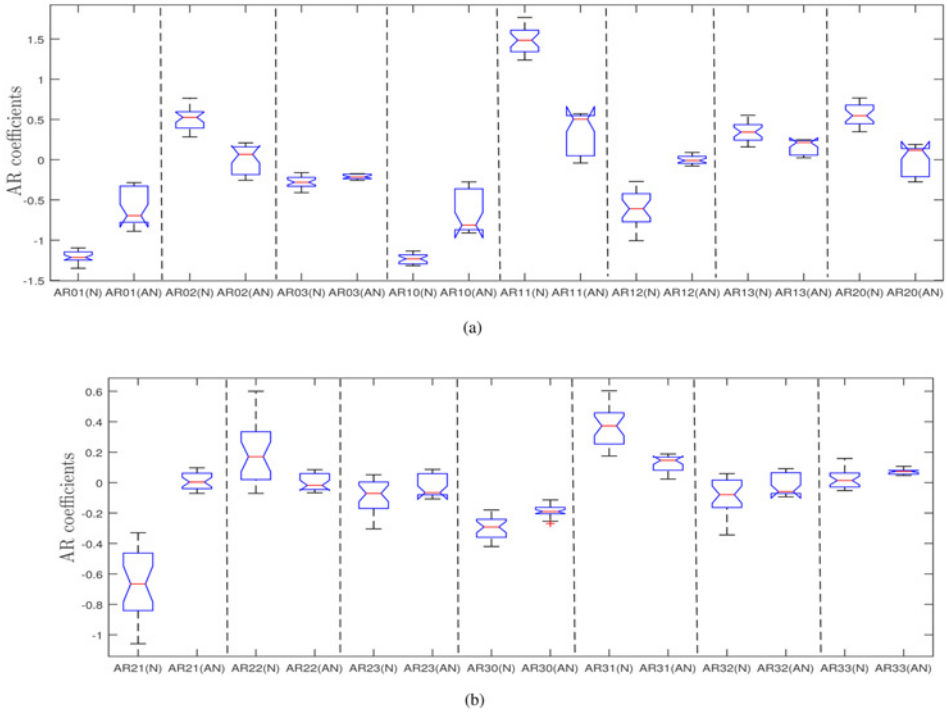

Fig. 7. Box plot of 3^{rd} order AR coefficients of normal and abnormal brain MR images: (a) AR01-AR20, (b) AR21-AR33.

As the *p*-values are very small, it can be concluded that AR coefficients as features are statistically significant and are effective for classification of normal and abnormal brain MR images. Finally, LS-SVM is employed for classification of brain MR images with AR coefficients as feature vector.

A set of experiments have been performed to investigate the performance of our approach with different orders of the AR model and different kernel functions of LS-SVM. Specifically, the performance of the proposed methodology is evaluated with linear, polynomial and RBF kernel functions in LS-SVM for 1^{st}, 2^{nd} and 3^{rd} order AR models. In addition, in order to study the effect of kernel parameters on the classification accuracy, we performed experiments by varying the degree of the polynomial kernel from 2 to 4 in steps of 1. Similarly, the σ value of RBF kernel function was varied from 0.1 to 10 in steps of 0.1. Specifically, we have performed 10-fold cross validation experiments.

Performance of the proposed method was evaluated using performance measures such as accuracy, sensitivity and specificity. Suppose *TP* and *TN* denote the number of correctly classified positive and negative samples and *FP* and *FN* denote the number of falsely classified negative and positive samples respectively. The performance measures are defined as follows [61]:

1. Accuracy (*ACC*): It is defined as the fraction of correctly classified positives and negative samples out of the total number of test samples and it is given as:

$$ACC = \frac{TP+TN}{TP+TN+FP+FN} \times 100 \tag{17}$$

2. Sensitivity (*SEN*): It is defined as the ratio of numbers of correctly classified positive samples to the total number to positive test samples and it is given as:

$$SEN = \frac{TP}{TP+FN} \times 100 \tag{18}$$

Table 2. *p*-values of AR coefficients obtained from Kruskal-Wallis test.

p-Value	1^{st} order	2^{nd} order	3^{rd} order
p_1	1.9×10^{-9}	1.32×10^{-9}	1.32×10^{-9}
p_2	3.43×10^{-9}	1.32×10^{-9}	1.32×10^{-9}
p_3	1.32×10^{-9}	1.32×10^{-9}	0.0007
p_4	-	1.32×10^{-9}	1.32×10^{-9}
p_5	-	1.32×10^{-9}	1.32×10^{-9}
p_6	-	1.32×10^{-9}	1.32×10^{-9}
p_7	-	1.32×10^{-9}	3.68×10^{-6}
p_8	-	0.0276	1.32×10^{-9}
p_9	-	-	1.32×10^{-9}
p_{10}	-	-	0.0005
p_{11}	-	-	0.079
p_{12}	-	-	3.878×10^{-7}
p_{13}	-	-	2.71×10^{-9}
p_{14}	-	-	0.0204
p_{15}	-	-	0.0022

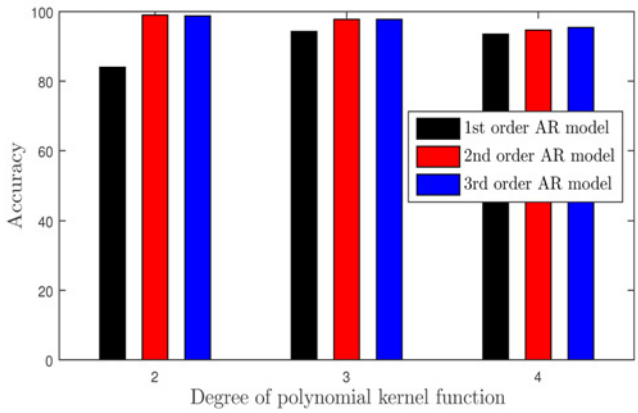

Fig. 8. Plot of classification accuracy versus degree of polynomial kernel function in LS-SVM.

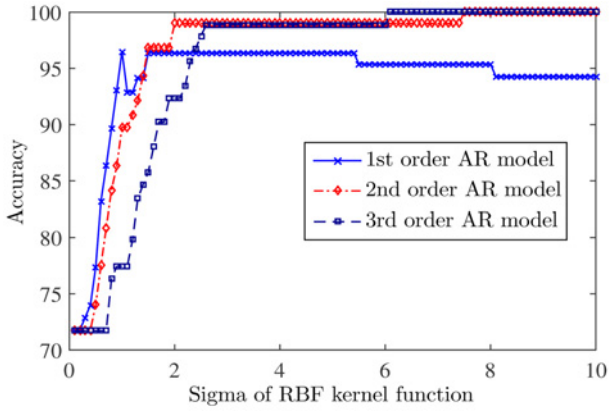

Fig. 9. Plot of classification accuracy versus sigma of RBF kernel function in LS-SVM.

3. Specificity (*SPF*): It is defined as ratio of number of correctly classified negative samples to the total number of negative test samples and it is given as:

$$SPF = \frac{TN}{TN+FP} \times 100 \tag{19}$$

A plot of classification accuracy versus degree of polynomial kernel function in LS-SVM is shown in Fig. 8, from which it can be observed that 1^{st} order AR model provides the least classification accuracy consistently for 2^{nd}, 3^{rd} and 4^{th} degree polynomial kernel function. On the other hand, 2^{nd} and 3^{rd} order AR models achieve maximum accuracy for 2^{nd} degree of polynomial kernel function in LS-SVM.

Fig. 9 presents a plot of classification accuracy versus sigma values for RBF kernel function in LS-SVM obtained by varying σ values from 0.1 to 10. It can be observed from the Fig. 9 that accuracy of 1^{st} order AR model varies significantly for different values of σ and the accuracy decreases as σ value is increased. 1^{st} order AR model achieves accuracy less than 97% for all values of σ, whereas 2^{nd} order AR model achieves 100% accuracy for σ values greater than 8 and 3^{rd} order AR model achieves 100% accuracy for σ values greater than 6.5. Thus, it can be concluded that 3^{rd} order AR model achieves the maximum accuracy for the least value of σ.

The results of our experiments using 10-fold cross validation method are summarized in the Table 3. From the results, it is observed that the 2^{nd} order linear and RBF kernel function achieves 100% accuracy, sensitivity and specificity. Polynomial function achieves a maximum classification accuracy of 99% for 2^{nd} degree polynomial and 2^{nd} order AR model. Also it can be noticed that in the case of 2^{nd} order AR model, linear kernel function provides better accuracy as compared to polynomial (non-linear) kernel function. This may be due to overfitting, which occurs when model is excessively complex and size of training dataset is too small in comparison to model complexity. Overfitting can be considered as a situation when model begins to memorize training data rather than learning to generalize from the trend. Due to small number of samples for each abnormal class in the database, partitioning of the database for 10-fold cross validation might result in very few abnormal samples in some of the subsets. In order to address this concern, experiments are also performed using 2-fold and 3-fold cross validation methods and results are summarized in Tables 4 and 5 respectively. It may be observed that performance trend remains similar, achieving 100% accuracy consistently for 2^{nd} and 3^{rd} order RBF kernel functions.

The performance of the proposed methodology is compared with that of the existing approaches on the same database and the classification accuracy is shown in Table 6. In the literature, different approaches have been used to partition the dataset for classification. Some of the existing methods used fixed approach, in which some percentage of the data is used for training and remaining data is used for testing. However, the percentage of the data used for training and testing vary from method to method. Other existing works used leave-one-out method (LOOM). The proposed work has been evaluated using the standard 10-fold cross validation method. In addition, we present classification accuracy of our method using LOOM for a fair comparison with some of the existing works. It can be observed that proposed method outperforms the existing methods, specifically our results are better than the 1D-EMD based approach presented in [18]. It is also important to note that the approach based on 1D-EMD achieved 99% when evaluated using leave-one-out method, which tends to result in higher accuracy than 10-fold cross validation. A major drawback of the 1D-EMD based technique for MR image classification is that it requires vectorization of the image before decomposition. In the process, important spatial information (including spatial frequency and correlation) is completely lost. This is a

Table 3. Performance of the proposed approach for classification of brain MR images using 10-fold cross validation.

Order of AR model	kernel	Accuracy	Sensitivity	Specificity
1^{st}	Polynomial	94.27	95.23	96.66
1^{st}	Linear	93.30	95.47	100
1^{st}	RBF	96.63	90.70	100
2^{nd}	Polynomial	99	98.57	86.67
2^{nd}	Linear	100	100	100
2^{nd}	RBF	100	100	100
3^{rd}	Polynomial	98.75	98.33	90.00
3^{rd}	Linear	97.63	96.66	90
3^{rd}	RBF	100	100	100

Table 4. Performance of the proposed approach for classification of brain MR images using 2-fold cross validation.

Order of AR model	kernel	Accuracy	Sensitivity	Specificity
1^{st}	Polynomial	94.39	95.26	96.15
1^{st}	Linear	88.47	84	100
1^{st}	RBF	96.50	100	100
2^{nd}	Polynomial	96.59	98.39	91.98
2^{nd}	Linear	100	100	100
2^{nd}	RBF	100	100	100
3^{rd}	Polynomial	98.86	95.16	96.15
3^{rd}	Linear	96.6	95.30	100
3^{rd}	RBF	100	100	100

Table 5. Performance of the proposed approach for classification of brain MR images using 3-fold cross validation.

Order of AR model	kernel	Accuracy	Sensitivity	Specificity
1^{st}	Polynomial	92.07	95.24	87.96
1^{st}	Linear	95.44	93.65	100
1^{st}	RBF	96.63	100	100
2^{nd}	Polynomial	98.85	100	100
2^{nd}	Linear	97.70	96.82	100
2^{nd}	RBF	100	100	100
3^{rd}	Polynomial	98.85	100	100
3^{rd}	Linear	97.70	96.82	100
3^{rd}	RBF	100	100	100

Table 6. Comparison of the proposed methodology with the existing methods studied on the same database.

Methodology	Classification approach	Accuracy
DWT and SOM [5]	Fixed partition	94
DWT and SVM [5]	Fixed partition	98
DWT, PCA and ANN [12]	Fixed partition	97
DWT, PCA and k-PNN [12]	Fixed partition	98
DWT, PCA and BPNN [6]	Fixed partition	100
DWT, Entropy and SVM [18]	LOOM	97
EMD, Entropy and SVM [18]	LOOM	99
Proposed approach	10-fold cross validation	100
Proposed approach	LOOM	100

plausible explanation for superior performance of our approach as compared to 1D-EMD based approach.

CONCLUSION

In this work, we have proposed a new method based on the bi-dimensional empirical mode decomposition (BEMD) for classification of magnetic resonance (MR) brian images. The features extracted from the autoregressive (AR) model of bi-dimensional intrinsic mode functions (IMFs) have been proposed for classification of brain MR images. The least-squares support vector machine (LS-SVM) together with radial basis function (RBF) kernel function has provided maximum classification accuracy for classification of brain MR images. In the proposed method, the kernel parameters have been selected based on the trial and error method. In future, it would be of interest to develop an automatic strategy for selecting kernel parameters and kernel function. The proposed technique for classification of brain MR images has been studied on limited database. It is necessary to study proposed methodology on large database before applying this for clinical purpose.

CONFLICT OF INTEREST STATEMENTS

Sahu O declares that he has no conflict of interest in relation to the work in this article. Anand V declares that he has no conflict of interest in relation to the work in this article. Kanhangad V declares that he has no conflict of interest in relation to the work in this article. Pachori RB declares that he has no conflict of interest in relation to the work in this article.

REFERENCES

[1] Kumar EP, Sumithra MG, Kumar PS. Abnormality detection in brain MRI/CT using segmentation algorithm and 3D visualization. Conf Proc Int Conf Adv Comput. 2013; 1:56-62.
[2] Nandpuru HB, Salankar SS, Bora VR. MRI brain cancer classification using support vector machine. Conf Proc IEEE Std Conf Electr Electron Comput Sci. 2014; 1:1-6.
[3] Lahmiri S, Boukadoum M. Automatic detection of Alzheimer disease in brain magnetic resonance images using fractal features. Conf Proc IEEE/EMBS Neural Eng. 2013; 1:1505-8.
[4] Blonda P, Satalino G, Baraldi A, De Blasi R. Segmentation of multiple sclerosis lesions in MRI by fuzzy neural networks: FLVQ and FOSART. Conf Proc Conf North American Fuzzy

Information Process Soc. 1998; 1:39-43.
[5] Chaplot S, Patnaik LM, Jagannathan NR. Classification of magnetic resonance brain images using wavelets as input to support vector machine and neural network. Biomed Signal Process Control. 2006; 1(1):86-92.
[6] Zhang Y, Dong Z, Wu L, Wang S. A hybrid method for MRI brain image classification. Expert Syst Appl. 2011; 38(8):10049-53.
[7] Lahmiri S, Boukadoum M. Hybrid discrete wavelet transform and gabor filter banks processing for features extraction from biomedical images. J Med Eng. 2013; doi: 10.1155/2013/104684.
[8] Abdullah N, Ngah UK, Aziz SA. Image classification of brain MRI using support vector machine. Conf Proc IEEE Int Conf Imaging Syst Tech. 2011; 1:242-7.
[9] Fletcher-Heath LM1, Hall LO, Goldgof DB, Murtagh FR. Automatic segmentation of non-enhancing brain tumors in magnetic resonance images. Artif Intell Med. 2001 Jan-Mar; 21(1-3):43-63.
[10] Maitra M, Chatterjee A. Hybrid multiresolution Slantlet transform and fuzzy c-means clustering approach for normal pathological brain MR image segregation. Med Eng Phys. 2008; 30(5):615-23.
[11] Htike KK, Khalifa OO. Comparison of supervised and unsupervised learning classifiers for human posture recognition. Conf Proc Int Conf Comput Commun Eng. 2010; 1:1-6.
[12] El-Dahshan ES, Hosny T, Salem ABM. Hybrid intelligent techniques for MRI brain images classification. Digit Signal Process. 2010; 20(2):433-41.
[13] Hackmack K, Paul F, Weygandt M, Allefeld C, Haynes JD. Multi-scale classification of disease using structural MRI and wavelet transform. Neuroimage. 2012; 62(1):48-58.
[14] Kalbkhani H, Shayesteh MG, Zali-Vargahan B. Robust algorithm for brain magnetic resonance image (MRI) classification based on GARCH variances series. Biomed Signal Process Control. 2013; 8(6):909-19.
[15] Maitra M, Chatterjee A. A Slantlet transform based intelligent system for magnetic resonance brain image classification. Biomed Signal Process Control. 2006; 1(4):299-306.
[16] Saritha M, Joseph KP, Mathew AT. Classification of MRI brain images using combined wavelet entropy based spider web plots and probabilistic neural network. Pattern Recognit Lett. 2013; 34(16):2151-6.
[17] Lahmiri S, Boukadoum M. Brain MRI classification using an ensemble system and LH and HL wavelet sub-bands features. Conf Proc IEEE Int Workshop Comput Intell Med Imaging. 2011; 1:1-7.
[18] Lahmiri S, Boukadoum M. An application of the empirical mode decomposition to brain magnetic resonance images classification. Conf Proc IEEE Latin American Symp Circuit Syst. 2013; 1:1-4.
[19] El-Dahshan ES, Mohsen HM, Revett K, Salem AB. Computer-aided diagnosis of human brain tumor through MRI: A survey and a new algorithm. Expert Syst Appl. 2014; 41(11):5526-45.
[20] Huang NE, Shen Z, Long SR, Wu MC, Shih HH, Zheng Q, Yen NC, Tung CC, Liu HH. The empirical mode decomposition and the hilbert spectrum for nonlinear and non-stationary time series analysis. Proc Conf R Soc Lond. 1998; 454(4):903-95.
[21] Flandrin P, Rilling G, Goncalves P. Empirical mode decomposition as a filter bank. IEEE Signal Process Lett. 2004; 11(2):112-4.
[22] Nunes JC, Bouaoune Y, Delechelle E, Niang O, Bunel Ph. Image analysis by bidimensional empirical mode decomposition. Image Vision Comput. 2003; 21(12):1019-26.
[23] Kumar TS, Kanhangad V, Pachori RB. Classification of seizure and seizure-free EEG signals using multi-level local patterns. Conf Proc Int Conf Digit Signal Process. 2014; 1:646-50.
[24] Pachori RB. Discrimination between ictal and seizure-free EEG signals using empirical mode decomposition. Res Lett Signal Process. 2008; doi: 10.1155/2008/293056.
[25] Pachori RB, Sharma R, Patidar S. Classification of normal and epileptic seizure EEG signals based on empirical mode decomposition. Complex Syst Model Control Intell Soft Comput. 2015; 319:367-88.
[26] Sharma R, Pachori RB, Acharya UR. Application of entropy measures on intrinsic mode functions for the automated identification of focal electroencephalogram signals. Entropy. 2015; 17(2):669-91.
[27] Pachori RB, Patidar S. Epileptic seizure classification in EEG signals using second-order difference plot of intrinsic mode functions. Comput Methods Programs Biomed. 2014; 113(2):494-502.
[28] Sharma R, Pachori RB. Classification of epileptic seizures in EEG signals based on phase space representation of intrinsic mode functions. Expert Syst Appl. 2015; 42(3):1106-17.
[29] Pachori RB, Bajaj V. Analysis of normal and epileptic seizure EEG signals using empirical mode decomposition. Computer Methods Programs Biomed. 2011; 104(3):373-81.
[30] Parey A, Pachori RB. Variable cosine windowing of intrinsic modefunctions: Application to gear fault diagnosis. Measurement. 2012; 45(3):415-26.
[31] Pachori RB, Hewson D, Snoussi H, Duchene J. Postural time-series analysis using empirical mode decomposition and second-order difference plots. Conf Proc IEEE Int Conf Acoust Speech Signal Process. 2009; 1:537-40.
[32] Huang H, Pan J. Speech pitch determination based on Hilbert-Huang transform. Signal Process. 2006; 86(4):792-803.
[33] Nunes JC, Guyot S, Delchelle E.Texture analysis based on local analysis of the bidimensional empirical mode decomposition. Machin Vis Appl. 2005; 16(3):177-88.
[34] Soille P. Morphological image analysis: principles and applications. 2nd ed. Berlin Heidelberg: Springer-Verlag; 2004.
[35] Carr JC, Fright WR, Beatson RK. Surface interpolation with radial basis functions for medical imaging. IEEE Trans Med Imaging. 1997; 16(1):96-107.
[36] Nunes JC, Niang O, Bouaoune Y, Delechelle E, Bunel Ph. Texture analysis based on the bidimensional empirical mode decomposition with gray-level co-occurrence models. Conf Proc Int Symp Singal Process Appl. 2003; 2:633-5.
[37] Qiao L-H, Guo W, Yuan W-T, Niu K-F, Peng L-Z. Texture analysis based on bidimensional empirical mode decomposition and quaternions. Conf Proc Int Conf Wavelet Anal Pattern Recognit. 2009; 1:84-90.
[38] Bhuiyan SMA, Adhami RR, Ranganath HS, Khan JF. Aurora image denoising with a modified bidimensional empirical mode decomposition method. IEEE Southeastcon. 2008; 1:527-32.
[39] Taghia J, Doostari MA, Taghia J. An image watermarking method based on bidimensional empirical mode decomposition. Conf Proc IEEE Congress Image Signal Process. 2008; 5:674-8.
[40] Chen WK, Lee JC, Han WY, Shih CK, Chang KC. Iris recognition based on bidimensional empirical mode decomposition and fractal dimension. Information Sci. 2013; (221):439-51.
[41] Ahmed MU, Mandic DP. Image fusion based on fast and adaptive bidimensional empirical mode decomposition. Proc 13th Conf on Information Fusion. 2010; 1-6.
[42] Wan J, Ren L, Zhao C. Image feature extraction based on the two-dimensional empirical mode decomposition. Conf Proc IEEE Congress Image Signal Process. 2008; 1:627-31.
[43] He Z, Wang Q, Shen Y, Jin J, Wang Y. Multivariate gray model-based BEMD for hyperspectral image classification. IEEE T Instrum Meas. 2013; 62(5):889-904.

[44] Ling L, Ming L, YuMing L.Texture classification and segmentation based on bidimensional empirical mode decomposition and fractal dimension. Conf Proc Int Workshop Educ Technol Comput Sci. 2009; 2:574-7.
[45] MATLAB central file exchange. ttp://www.mathworks.com/matlabcentral/fileexchange/28761-bi-dimensional-emperical-mode-decomposition--bemd-/content/bemd.m Accessed september 2014.
[46] Nam M, Lee Y. 2D AR (1,1) analysis of blurring image by empirical mode decomposition. Comput Appl Web Hum Comput Signal Image Process Pattern Recognit. 2012; 342:118-25.
[47] Dubois SR, Glanz FH. An autoregressive model approach to two-dimensional shape classification. IEEE T PATTERN ANAL. 1986; 8(1):55-66.
[48] Anderson CW, Stolz EA, Shamsunder S. Multivariate autoregressive models for classification of spontaneous electroencephalographic signals during mental tasks. IEEE Trans Biomed Eng. 1998; 45(3):277-86.
[49] Vuksanovic B, Alhamdi M. AR-based method for ECG classification and patient recognition. Int J Biom Bioinform. 2013; 7(2):74-92.
[50] Deguchi K. Two-dimensional auto-regressive model for analysis and sythesis of gray-level textures. Conf Proc Int Symp Sci Form.
[51] Vapnik VN. The nature of statistical learning theory. 2nd ed. Berlin Heidelberg: Springer-Verlag; 1995.
[52] Suykens J, Vandewalle J. Least squares support vector machine classifiers. Neural Process Lett. 1999; 9(3):293-300.
[53] Khandoker AH, Lai DT, Begg RK, Palaniswami M. Wavelet-based feature extraction for support vector machines for screening balance impairments in the elderly. IEEE Trans Neural Syst Rehabil Eng. 2007; 15(4):587-97.
[54] Bajaj V, Pachori RB. Classification of seizure and nonseizure EEG signals using empirical mode decomposition. IEEE Trans Inf Technol Biomed. 2012; 16(6):1135-42.
[55] Joshi V, Pachori RB, Vijesh A. Classification of ictal and seizure-free EEG signals using fractional linear prediction. Biomed Signal Process Control. 2014; 9:1-5.
[56] Polat K, Akdemir B, Gunes S. Computer aided diagnosis of ECG data on the least square support vector machine. Digit Signal Process. 2008; 18(1):25-32.
[57] Yan Z, You X, Chen J, Ye X. Motion classification of EMG signals based on wavelet packet transform and LS-SVMs ensemble. Trans Tianjin Univ. 2009; 15(4):300-7.
[58] Das S, Chowdhury M, Kundu MK. Brain MR image classification using multiscale geometric analysis of ripplet. Prog Electromagn Res. 2013; 137:1-17.
[59] AANLIB database of Harward medical school. http://www.med.harvard.edu/aanlib/. Accessed september 2014.
[60] Freund RJ, Mohr D, Wilson WJ. Statistical Methods. 3rd ed. San Diego: Academic Press; 2010.
[61] Azar AT, El-Said SA. Performance analysis of support vector machines classifiers in breast cancer mammography recognition. Neural Comput Appl. 2014; 24(5):1163-77.